Swift-Hohenberg equation with broken cubic-quintic nonlinearity

S. M. Houghton*
School of Mathematics, University of Leeds, Leeds LS2 9JT, United Kingdom

E. Knobloch†
Department of Physics, University of California, Berkeley, California 94720, USA

(Received 15 February 2011; published 7 July 2011)

The cubic-quintic Swift-Hohenberg equation (SH35) provides a convenient order parameter description of several convective systems with reflection symmetry in the layer midplane, including binary fluid convection. We use SH35 with an additional quadratic term to determine the qualitative effects of breaking the midplane reflection symmetry on the properties of spatially localized structures in these systems. Our results describe how the snakes-and-ladders organization of localized structures in SH35 deforms with increasing symmetry breaking and show that the deformation ultimately generates the snakes-and-ladders structure familiar from the quadratic-cubic Swift-Hohenberg equation. Moreover, in nonvariational systems, such as convection, odd-parity convectons necessarily drift when the reflection symmetry is broken, permitting collisions among moving localized structures. Collisions between both identical and nonidentical traveling states are described.

DOI: 10.1103/PhysRevE.84.016204 PACS number(s): 05.45.−a, 47.54.−r, 47.20.Ky

I. INTRODUCTION

Recent studies of convection in binary fluids, both in bulk mixtures [1,2] and in porous media [3], have identified states of spatially localized convection that have been called convectons [4]. Related states are also present in convection in a magnetic field [4,5], in natural doubly diffusive convection [6,7], and in Marangoni convection [8]. These states are time independent and may form bound states called multipulse convectons. In two-dimensional systems with a midplane reflection symmetry, such as binary fluid convection, the midplane symmetry is responsible for the presence of two types of convectons with opposite parity: even-parity convectons that are invariant with respect to spatial reflection $R: x \to -x$ and odd-parity convectons, invariant under R followed by a midplane reflection $\kappa: z \to 1 - z$. Convectons of both types are present in a Rayleigh number regime called the snaking or pinning region located in the subcritical regime of the bifurcation diagram in which spatially periodic convection coexists with the conduction state. The term snaking refers to the back-and-forth oscillations of the convecton branches within this region as the convectons grow in length by nucleating new cells at either end. This process is captured well by a model partial differential equation on the real line, the Swift-Hohenberg equation, with competing cubic and quintic nonlinearities (hereafter, SH35),

$$u_t = ru - \left(1 + \partial_x^2\right)^2 u + b_3 u^3 - u^5. \tag{1}$$

Here, $u(x,t)$ is a real-valued order parameter. The equation defines an intrinsic length scale, here 2π, and is completely parametrized by the driving r and the cubic coefficient b_3.

The SH35 has two symmetries, $R: x \to -x$ and $\kappa: u \to -u$, completely analogous to the symmetries of two-dimensional binary fluid convection. The equation has been studied by a number of authors [9–11], and it is known that the snaking branches of even- and odd-parity localized states are braided and connected by additional links called rungs consisting of localized states with no parity. The resulting branch structure has been called the snakes-and-ladders structure of the snaking or pinning region [10]. Within SH35, the asymmetric states are also equilibria. This is a consequence of the variational (i.e., gradient) structure of the equation. However, all such asymmetric states are known to be unstable [10].

In the corresponding convection system, even-parity states are necessarily time independent. This is a consequence of their symmetry with respect to the symmetry R. In general, even-parity states of this type may undergo secondary bifurcations with increasing amplitude that break this symmetry producing a pair of symmetry-related asymmetric states. In a translation-invariant system posed on the real line (or with periodic boundary conditions in x), these states will, in general, travel, with the direction of travel and speed determined by the asymmetry. Bifurcations of this type are referred to as parity-breaking bifurcations [12]. The bifurcations to the rung states are pitchfork bifurcations of this type, implying that, in nonvariational systems, the rung states will, in general, travel, with a speed proportional to the square root of the distance from the bifurcation. The odd-parity convectons, also present in binary fluid convection, do not travel, however—these states are time independent like the even-parity states. This is a consequence of the symmetry $\kappa \circ R$ of these states, which forces the drift speed to vanish. Thus, odd-parity states also experience parity-breaking bifurcations leading to drift, provided the marginally stable eigenfunction breaks the symmetry $\kappa \circ R$. These bifurcations are responsible for the termination of the rung states within the snaking region on the branch of odd-parity states.

The above discussion implies that it is possible to make the odd-parity states drift by breaking the midplane reflection symmetry κ of the system. This can be achieved, for example, by using different boundary conditions at the top and bottom of the layer (on the velocity or temperature) or by incorporating non-Boussinesq effects into the description of the problem.

*smh@maths.leeds.ac.uk
†knobloch@berkeley.edu

These effects include temperature and concentration dependence of the transport coefficients or a quadratic dependence of the density on the temperature or concentration. One may also anticipate that the breaking of the symmetry κ should eliminate the distinction between the asymmetric rung states and the odd-parity states. Breaking the symmetry κ does not destabilize the even states and implies that, in systems with broken κ symmetry, one may study collisions among almost odd-parity states or among such states and the even-parity states, which remain stationary. The present paper is devoted to an exploration of these issues using Swift-Hohenberg-like model equations to serve as a guide for future studies of traveling convectons in binary fluid convection and related systems.

We study two systems with this property, the equation,

$$u_t = ru - \left(1+\partial_x^2\right)^2 u + b_3 u^3 - u^5 + \epsilon u^2, \tag{2}$$

and the equation,

$$u_t = ru - \left(1+\partial_x^2\right)^2 u + b_3 u^3 - u^5 + \epsilon (\partial_x u)^2. \tag{3}$$

Both equations contain a quadratic term that breaks the symmetry κ but respects the symmetry R; only one such term is included, the dominant one in powers of the amplitude, since its effects are believed to capture the essence of the breaking of the κ symmetry. Equation (2) continues to possess variational structure implying that both the R-symmetric states and the asymmetric states that result will continue to be stationary. This fact has numerous advantages for tracing out the effects of the symmetry-breaking term. However, in order to study the associated drifts alluded to above, we also study Eq. (3). We anticipate, and our computations confirm, that the replacement of the term ϵu^2 by the nonvariational term ϵu_x^2 has qualitatively similar consequences.

Throughout this paper, we set $b_3 = 2$ and solve the problem on a large domain with Neumann boundary conditions instead of solving it on an infinite domain. The results are found to be independent of the size of the domain provided the observed pattern is located in the center of the domain, far from the boundaries. All solutions are computed on the full domain, despite the fact that even solutions can be computed on the half domain and then reflected in $x = 0$ to find the solution on the full domain.

The usual snakes-and-ladders picture for SH35, Eq. (1), is shown in Fig. 1. There are three basic components to this figure: a snaking branch representing even-parity solutions, i.e., solutions invariant with respect to R, a snaking branch representing odd-parity solutions invariant with respect to $\kappa \circ R$, and the rung states. The rung states connect the two snaking branches, arising in pitchfork bifurcations close to the saddle-node bifurcations on the snaking branches. Moving up the snake, the saddle nodes themselves converge exponentially rapidly to fixed values of the parameter r and do so from the same side at both boundaries of the snaking region [13,14]. At the same time, the pitchfork bifurcations leading to the rung states converge exponentially rapidly to the saddle-node bifurcations [15,16].

Owing to the symmetry κ, each snaking branch represents two distinct solutions related by κ. We refer to even solutions with a maximum (minimum) in the center as L_0 (L_π).

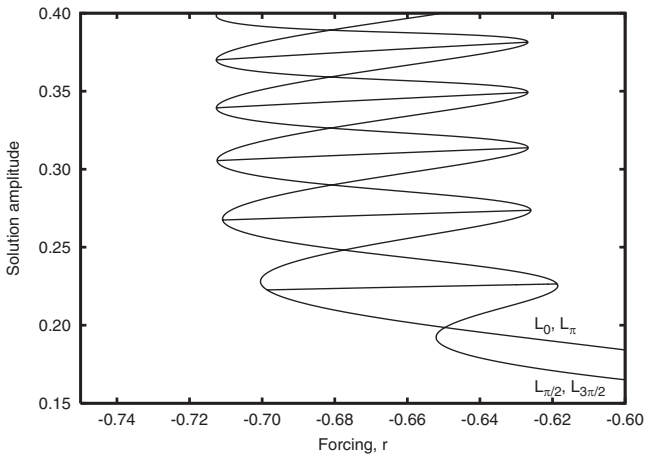

FIG. 1. The snakes-and-ladders structure of the pinning region $-0.713 < r < -0.626$ in SH35, Eq. (1), with $b_3 = 2$, $\epsilon = 0$.

Likewise, we refer to odd solutions with a negative (positive) slope in the center as $L_{\pi/2}$ ($L_{3\pi/2}$). In addition, each rung in the figure represents four distinct asymmetric states [11]. These facts will prove useful in what follows.

The solution amplitude is defined in terms of its normalized L_2 norm,

$$\mathcal{A} = \left[\frac{1}{L}\int_0^L u^2(x)dx\right]^{1/2}. \tag{4}$$

The normalization is included in order to compare the amplitude of localized states with that of the periodic state (which would otherwise have infinite amplitude as $L \to \infty$). However, because of the normalization, $\mathcal{A}$ vanishes for localized states on an infinite domain. To avoid this problem, all solution amplitudes quoted in the next two sections have been calculated on a domain of length 40π, i.e., 20 wavelengths of the basic pattern.

II. NUMERICAL STUDY OF EQ. (2)

A. Small symmetry breaking

Equation (2) is variational, like Eq. (1), and has a Lyapunov functional or *free energy* given by

$$\mathcal{F}[u(x)] = \frac{1}{L}\int_0^L \left\{ -\frac{1}{2}ru^2 + \frac{1}{2}\left[\left(1+\partial_x^2\right)u\right]^2 - \frac{1}{3}\epsilon u^3 - \frac{1}{4}b_3 u^4 + \frac{1}{6}u^6 \right\} dx. \tag{5}$$

Thus, the evolution of the system follows $u_t = -L\delta\mathcal{F}/\delta u$, and as a result, all solutions evolve as $t \to \infty$ toward local minima of the energy functional $\mathcal{F}$, i.e., to a time-independent state.

Figure 2 shows the solution branches in the snaking region when the symmetry κ of the problem is broken through setting $\epsilon = 0.03$ and compares the result with the snaking curves corresponding to the κ-symmetric case ($\epsilon = 0$), shown dashed. A number of changes can be seen.

The even solutions continue to snake but are split into two continuous branches. On the L_0 branch, the solution profiles continue to have maxima in the center. Sample profiles, at

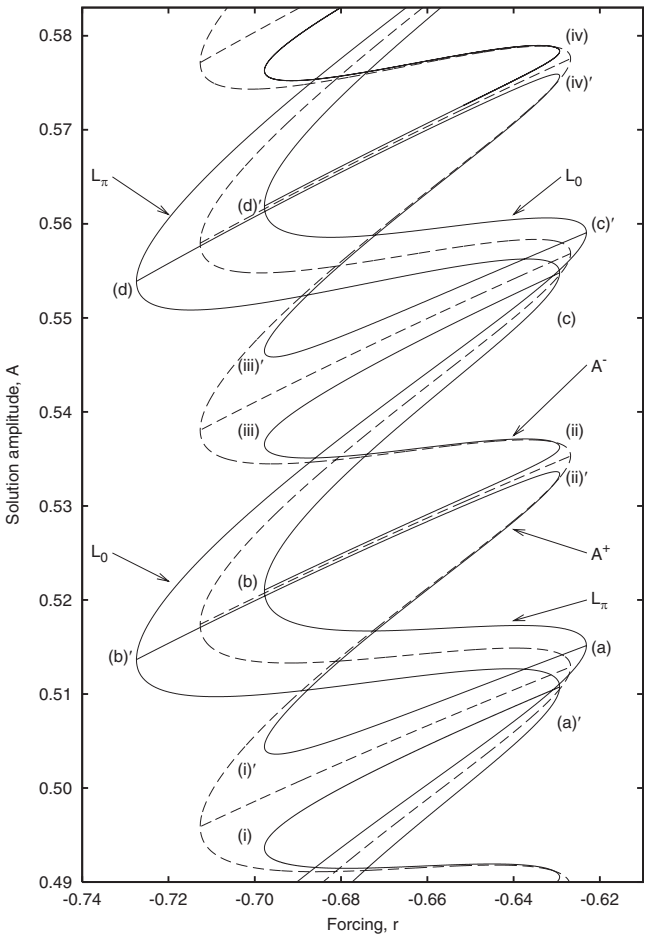

FIG. 2. As for Fig. 1, but with broken κ symmetry, $\epsilon = 0.03$. The snakes-and-ladders structure in the κ-symmetric case $\epsilon = 0$ is shown dashed. Solution profiles at the labeled saddle nodes are shown in Figs. 3 and 4.

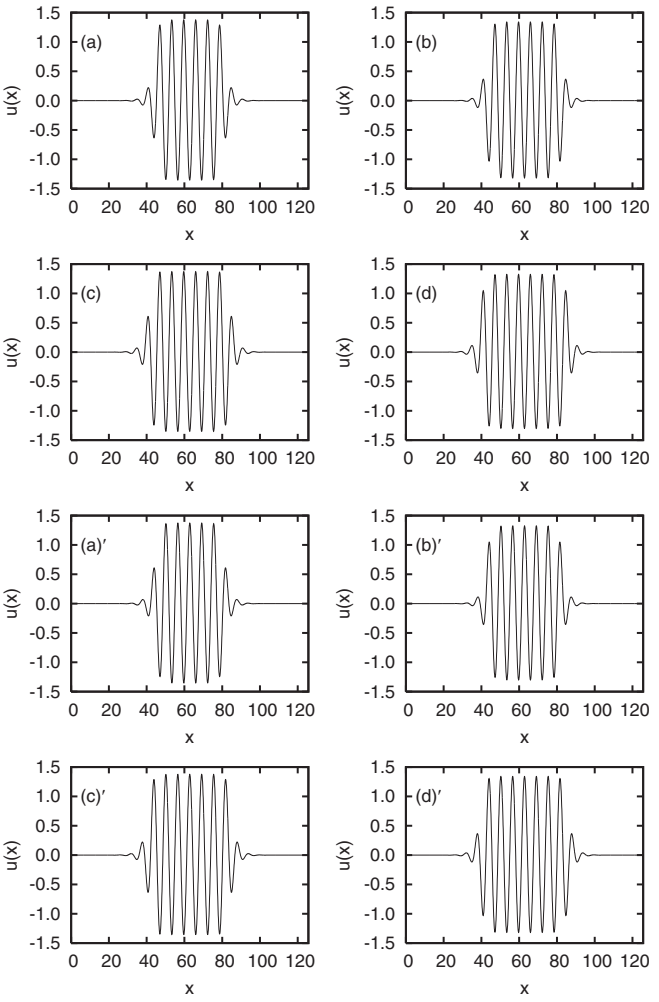

FIG. 3. Solution profiles $u(x)$ at the saddle nodes of Fig. 2. The profiles (a)–(d) are from the L_π branch while (a)′–(d)′ are from the L_0 branch.

locations labeled (a)′–(d)′ in Fig. 2, are shown in Fig. 3. On the L_π branch, the solution profiles have minima in the center. Sample profiles, labeled (a)–(d) in Fig. 2, are also shown in Fig. 3. In contrast, the breaking of the κ symmetry destroys the odd parity of states $L_{\pi/2}$, $L_{3\pi/2}$, producing two distinct asymmetric states $A^{\pm}$. Each of these states comes as a pair of states, related by the unbroken symmetry R, giving four asymmetric states altogether. As a result, the odd-parity branch does not split when $\epsilon \neq 0$ but instead breaks up into *disconnected* parts. In view of their shapes, we refer to these disconnected branches as S branches or Z branches. We first describe the even states in more detail, before discussing the S and Z branches.

When $\epsilon = 0$, the two even branches, L_0 and L_π, coincide, and the corresponding profiles are related by the symmetry κ. This symmetry is broken when $\epsilon \neq 0$ and results in the splitting of the L_0 and L_π branches. For $|\epsilon| \ll 1$, the splitting is on the order of $|\epsilon|^{1/2}$ (cf. Ref. [17]) and is most visible at each saddle node. As a result of the splitting, every second saddle node on the L_0 branch moves outward relative to the $\epsilon = 0$ branch while the corresponding saddle nodes on the L_π branch move inward. The opposite occurs at the saddle nodes in between. This behavior takes place along both the left and the right boundaries of the snaking region. As a result, there are now *four* values of r at which the folds on these branches accumulate, $r = -0.7274$ and $r = -0.6987$ on the left and $r = -0.6293$ and $r = -0.6231$ on the right. Thus, the broken κ symmetry leads to an *increase* in the overall width of the snaking region. Moreover, since the solutions on the L_0, L_π branches remain even, the parity-breaking bifurcations near each saddle node remain pitchforks and continue to be responsible for the bifurcation of spatially asymmetric states from these branches. Thus, each rung in the diagram is split into two branches, one of which forms a part of an S branch while the other forms a part of a Z branch, each of which continues to represent a pair of asymmetric localized states related by the symmetry R.

Specifically, the solution labeled (a) at the right boundary of the snaking region is an L_π solution that results from an outward displacement of the saddle node, while the next saddle node on the right, labeled (c), is displaced inward. The solution (c) has a pair of extra down cells on either side, implying that the fronts in (c) are mirror images of those in (a). Therefore, it is necessary to proceed one more wavelength up the snake before one recovers a solution resembling (a) but with a full extra

wavelength on either side of the structure. Similar evolution takes place along the L_0 branch. We see that the L_0 solution (a)′ is displaced inward, while the next L_0 state above, labeled (c)′, is displaced outward. This time, proceeding up the L_0 branch from state (a)′ to state (c)′ results in the addition of a pair of up cells, one on each side, while the down cells saturate in amplitude. In proceeding from (c)′ to (e)′, not shown, the structure adds a pair of down cells on either side while the existing up cells saturate.

These observations can be interpreted in terms of nucleation of new cells, either up cells or down cells, at the front and back of the localized structure as one follows each branch. This nucleation takes place at the left boundary of the snaking region, where the cells bounding the localized structure are weakest. For example, a down cell is nucleated at (b)′ on the outside of a reduced strength up cell, while an up cell is nucleated at (d)′ on the outside of a reduced strength down cell; by the time one reaches the right boundary at (c)′, the reduced strength up cells have grown to full strength, and the new down cells have grown to half strength. Because of the weakness of the cells in the nucleation region, this region is affected the most by the symmetry breaking and, hence, exhibits the largest splitting. Which way a branch shifts depends on whether one is adding cells that are favored by the symmetry breaking in which case the saddle node shifts outward, or cells that are opposed by the symmetry breaking in which case the saddle node shifts inward. For sufficiently small ϵ, the resulting shifts are equal and opposite for the L_0, L_π branches. A similar discussion applies at the right boundary, although the magnitude of the shift is reduced. This is a consequence of the fact that the symmetry breaking has a smaller effect on fully developed cells. All shifts are reversed when the sign of ϵ is reversed.

Figure 4 shows the solution profiles at saddle nodes on the disconnected S and Z branches. As already mentioned, the odd-parity branch does not split when $\epsilon \neq 0$ but instead, breaks up into *disconnected* parts. This is a direct consequence of the fact that once $\epsilon \neq 0$, the resulting states have no parity. As a result, the pitchfork bifurcations, present near each saddle node when $\epsilon = 0$, are unfolded, resulting in a continuous transition between states resembling $L_{\pi/2,3\pi/2}$ and one or other of the states $A^{\pm}$ on the former rung states. Figure 2 shows that these reconnections result in two types of branches of asymmetric states, S branches [e.g., (b)–(ii)–(iii)–(c)], and Z branches [e.g., (a)–(i)′–(ii)′–(b)′]. The S branches provide connections from an L_0, or L_π, branch back to itself, while the Z branches provide interconnections between the L_0 and L_π branches. The folds on these branches all align with the inner folds on the L_0, L_π branches, i.e., at $r = -0.6987$ and $r = -0.6293$. In contrast to the even branches, all folds on the $L_{\pi/2}$ and $L_{3\pi/2}$ branches are displaced slightly inward when $\epsilon \neq 0$, and this is so both at the left and the right boundaries of the snaking region. This is because adding an up cell at one end of an odd-parity state and a down cell at the other generates an intermediate saddle-node displacement.

States on the S and Z branches, such as (i) and (i)′, are related by approximate κ symmetry. Comparison of profile (i) in Fig. 4 with the image of (iii) under R shows that, in proceeding upward from one S branch to the next, one up cell and one down cell are added to the solution profile, i.e., one

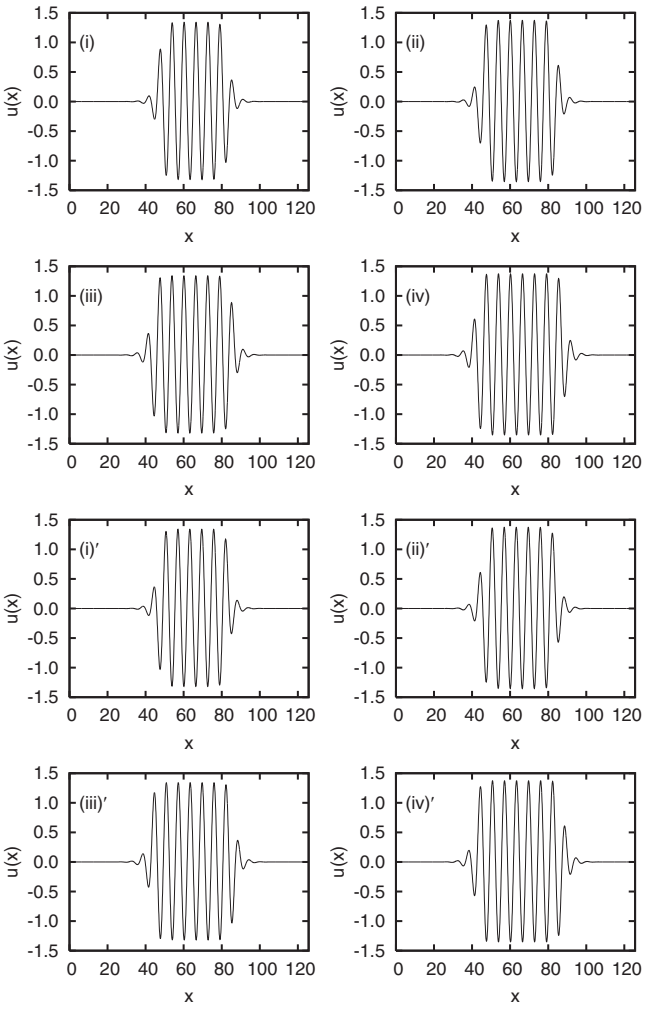

FIG. 4. Solution profiles $u(x)$ at the saddle nodes of the disconnected branches in Fig. 2. The profiles (i)–(iv) are from S branches while (i)′–(iv)′ are from Z branches.

extra wavelength. The same process occurs for the Z branches, for example, between (i)′ and the image of (iii)′ under R. Figures 3 and 4 also allow us to trace the evolution of the profiles along the S and Z branches. For example, in proceeding from profile (b) to profile (c) along the connecting S branch, we see that, between (b) and (ii), the up and down cells at the left shrink while those at the right both grow. Between (ii) and (iii), the cells at both ends grow, while between (iii) and (c), the cells at the left grow while those at the right shrink. The net effect of these changes is to increase the amplitude of the cells at either end, without changing the internal structure of the solution. In contrast, when proceeding from (a) to (b)′ along a Z branch, we see that, between (a) and (i)′, the cells at the left grow while those at the right shrink. Both sets grow between (i)′ and (ii)′ while between (ii)′ and (b)′, the cells at the left continue to grow while those at the right slightly shrink. The net effect of these changes is to add one wavelength to the structure, thereby turning an L_π state into an L_0 state.

In all cases, the length of the localized structure changes by one wavelength as one proceeds up the snaking structure in Fig. 2 from one fold to the next like fold.

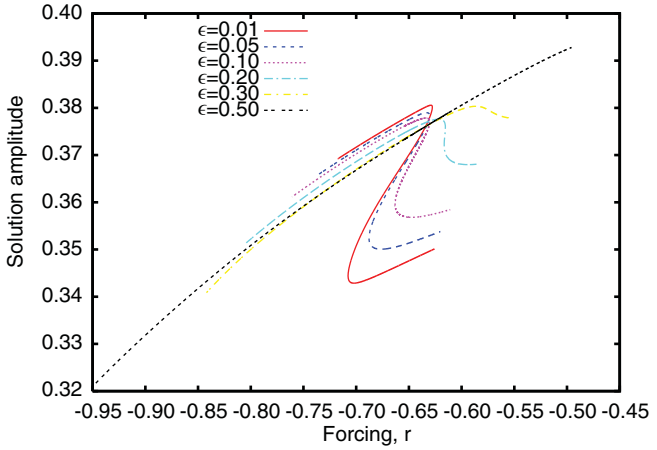

FIG. 5. (Color online) Evolution of a Z branch with ϵ. The central segment of each Z branch is stable while the upper and lower segments each have one real unstable eigenvalue.

B. Increased symmetry breaking

Figure 5 shows the effect of increasing the strength ϵ of the symmetry-breaking term on the width and shape of a particular Z branch of asymmetric states. The end points of each curve correspond to its termination on the L_0 and L_π branches. Thus, the end points are proxies for the location of the outermost saddle-node bifurcations while the saddle nodes define the boundaries of the inner snaking region. As shown in Fig. 5, as ϵ increases, the saddle nodes annihilate each other and so gradually straighten the Z shape into a monotonic curve.

The stability of the Z branch carries over from the $\epsilon = 0$ case. The upper and lower segments are unstable with one positive real eigenvalue, a consequence of the instability of the rung states when $\epsilon = 0$. However, the central segment is stable (when it exists) since this part of the curve is always the remnant of a *stable* segment of an $L_{\pi/2}$ ($L_{3\pi/2}$) branch.

As ϵ is increased, the S branches shrink in size as shown in Fig. 6 and disappear for $\epsilon > 0.2$. All solution profiles

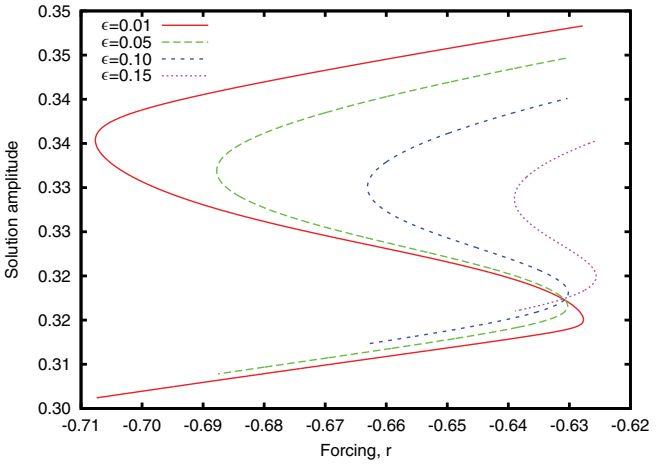

FIG. 6. (Color online) Evolution of an S branch with ϵ. For $\epsilon > 0.20$, S branches no longer exist. All states on these branches are unstable, with one real unstable eigenvalue on the sections with positive gradient and two real unstable eigenvalues on the sections with negative gradient.

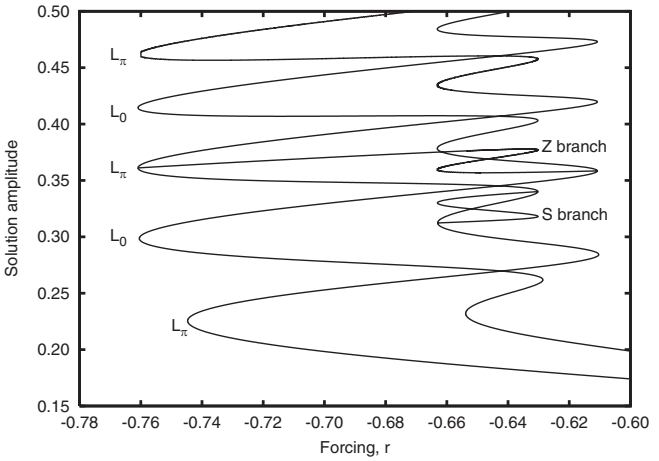

FIG. 7. Snaking region at $\epsilon = 0.1$. One Z-shaped rung and an S-shaped rung are included, taken from Figs. 5 and 6, respectively.

on S branches are unstable. As before, the upper and lower segments have a single real unstable eigenvalue, but this time, the central segment has two real unstable eigenvalues. This is a consequence of the fact that these segments are created from *unstable* segments of the $L_{\pi/2}$ ($L_{3\pi/2}$) branch when $\epsilon = 0$.

Stability properties along the snaking branches L_0, L_π also carry over from the $\epsilon = 0$ case: The segments of either branch sloping up from left to right are stable while the remaining segments are unstable. The cumulative effect of these changes is shown in Figs. 7 and 8.

III. NUMERICAL STUDY OF EQ. (3)

In this section, we examine the corresponding properties of the nonvariational system (3). As the solutions may now drift, we seek stationary solutions in a moving frame, i.e., $u(x,t) = u(\xi)$ with $\xi = x - ct$ and solve

$$0 = ru - \left(1 + \partial_\xi^2\right)^2 u + b_3 u^3 - u^5 + \epsilon(\partial_\xi u)^2 + c\partial_\xi u, \quad (6)$$

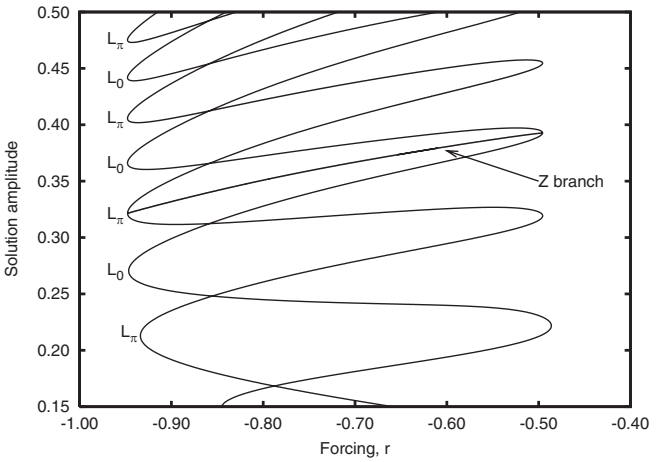

FIG. 8. Snaking region at $\epsilon = 0.5$. One Z-shaped rung, now straightened, is included, the same as shown in Fig. 5. For this value of ϵ, S branches are no longer present.

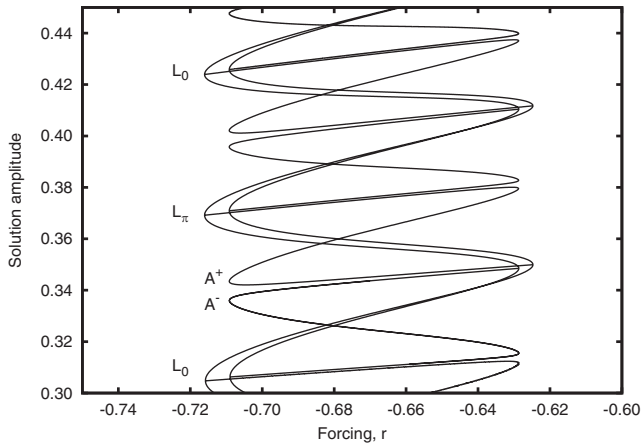

FIG. 9. Snaking region for Eq. (3) when $\epsilon = 0.01$, including all S and Z branches.

where c is treated as an (nonlinear) eigenvalue and is calculated as part of the solution. The symmetry R takes solutions $u(\xi; c)$ into solutions $u(-\xi; -c)$.

Figures 9–12 show that the symmetry breaking has essentially the same effect on the $\epsilon = 0$ snaking branches as in the variational case, and that with increasing ϵ, the S branches of asymmetric states gradually disappear while the Z branches gradually straighten. Thus, the net outcome of this behavior is to eliminate every second saddle node, both at the left and the right boundaries of the snaking region, and to replace the single snaking branch of even-parity states by a pair of braided L_0, L_π branches.

As in the variational case, solution stability carries over from SH35. As a result, the parts of the snaking curves sloping upward from left to right are stable while all other solutions are unstable. No oscillatory bifurcations have been found, although for $\epsilon = 0.3$, complex conjugate pairs of $L_{0,\pi}$ eigenvalues approach the imaginary axis close to the saddle nodes. We mention that, in the generic situation, the interaction of a saddle-node bifurcation with a parity-breaking bifurcation is expected to generate oscillations [18] and such oscillations

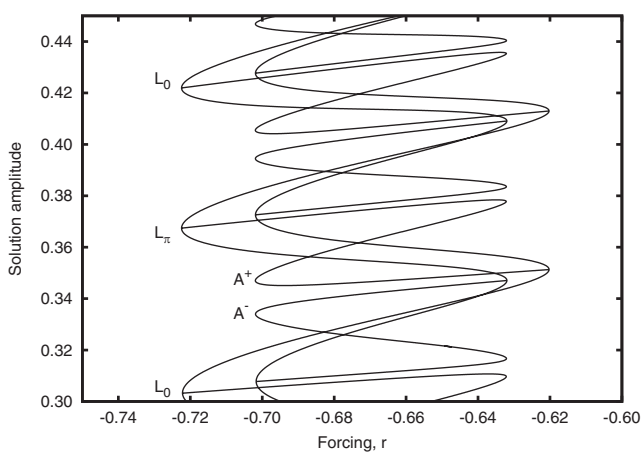

FIG. 10. Snaking region for Eq. (3) when $\epsilon = 0.03$, including all S and Z branches, for comparison with Fig. 2, also computed for $\epsilon = 0.03$.

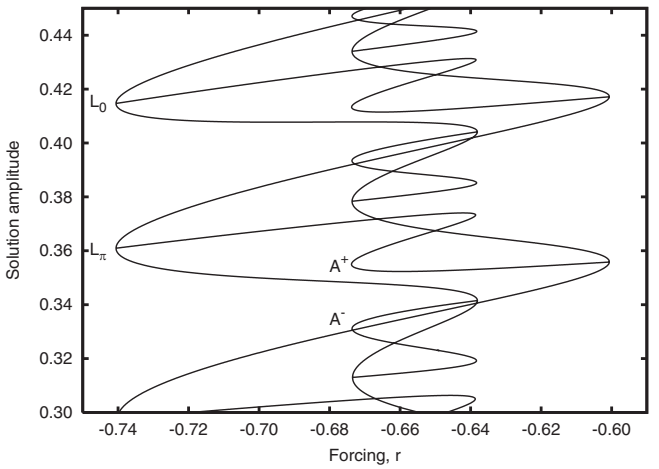

FIG. 11. Snaking region for Eq. (3) when $\epsilon = 0.1$, including all S and Z branches, for comparison with Fig. 7. The drift speed on the S branches passes through zero, while that along the Z branches maintains a constant sign.

are indeed present in the Swift-Hohenberg equation with sufficiently large nonvariational terms [19].

Figure 13 shows the S and Z branches of asymmetric states extracted from Fig. 9 for $\epsilon = 0.01$. As before, the end points are proxies for the outermost saddle nodes within the snaking region while the interval between the saddle nodes defines the inner snaking region in Fig. 9. The branches are drawn using distinct line types to facilitate comparison with Fig. 14 showing the drift speed c along these branches. Comparison of the figures reveals that the drift speed passes through zero along the S branches but remains of one sign along the Z branches. The reason for this is simple to understand. When proceeding from a left saddle node upward to a right saddle node, the cells at either end of the localized structure strengthen, thereby monotonically increasing the drift speed. However, along segments that extend upward from a right saddle node to a left saddle node, the incipient nucleation counteracts the drift as the asymmetry of the structure starts to reverse, and the drift must pass through zero before it starts building up past

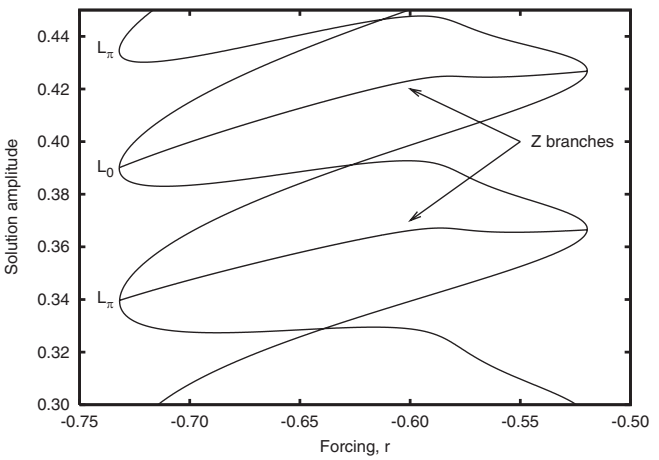

FIG. 12. Snaking region for Eq. (3) when $\epsilon = 0.3$. The S branches are now absent while the Z branches have straightened into rung states.

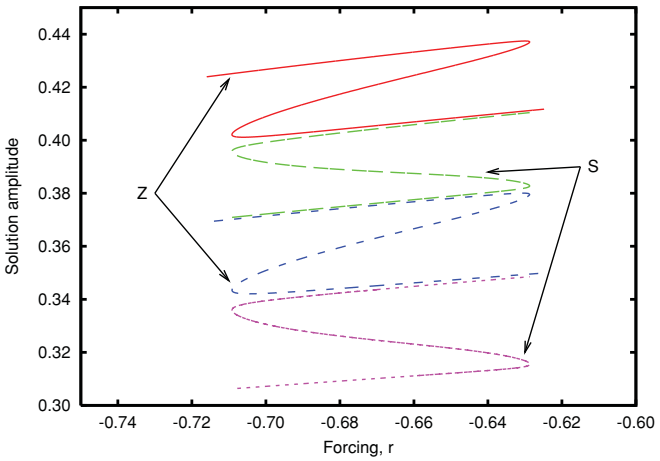

FIG. 13. (Color online) S and Z branches of asymmetric states from Fig. 9 for $\epsilon = 0.01$.

the left saddle node. Thus, the speed c changes sign along any branch that follows a segment of odd-parity states with a negative slope, i.e., on S branches. In contrast, the speed will be monotonic on any branch involving a segment with a positive slope, i.e., Z branches. Drift speeds are expected to decrease with increasing length of the localized state as the cells at either end that produce the drift become a smaller and smaller fraction of the state. This prediction is consistent with the computed maximum drift speeds in Fig. 14, e.g., the red (solid) and blue (dashed) curves in the figure.

IV. COLLISIONS OF TRAVELING LOCALIZED STATES

In this section, we explore the dynamics associated with the interaction between localized states of Eq. (3). All states are taken from stable sections of the solution branches at $r = -0.65$ and $\epsilon = 0.1$. We study, in turn, the interaction between two identical localized states traveling in opposite directions (head-on collision) and the interaction between two different localized structures selected from different Z branches but at the same value of r. When considering collisions between different structures, we describe separately the case in which

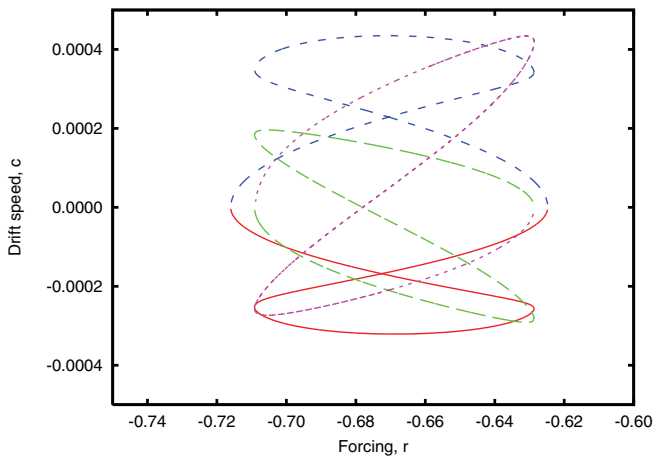

FIG. 14. (Color online) Drift speeds along the S and Z branches shown in Fig. 13. Line styles are consistent between these figures. The speeds reverse along S branches but are monotonic along Z branches.

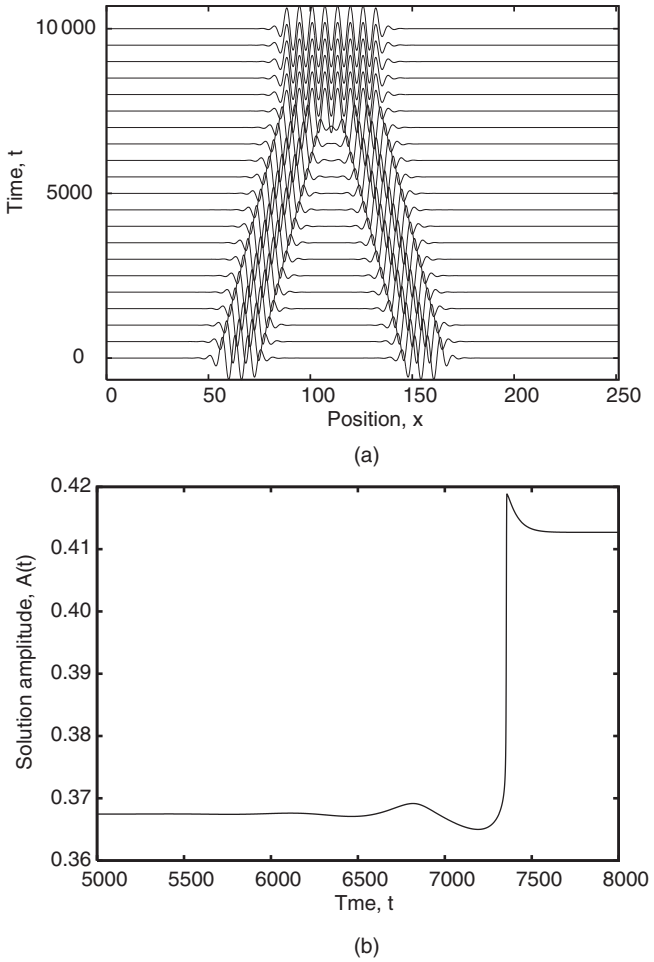

FIG. 15. (a) A head-on collision between two identical localized states u and Ru at $r = -0.65$ and $\epsilon = 0.1$, shown in the form of a space-time plot. When far apart, each pulse drifts with speed 4.2×10^{-3}. Solution profiles are separated by 500 time units. (b) Evolution of the solution amplitude $\mathcal{A}$, computed on the full domain of length 80π. The final state is a stationary even-parity localized state.

the structures are moving in the same direction and the case in which they move in opposite directions. We also consider collisions between an asymmetric traveling localized state and an even-parity stationary state.

We start with a head-on collision between an asymmetric state and its image under R, initially far apart, treated as an initial value problem. Far apart, the drift speed of each state is $c = 4.2 \times 10^{-3}$. The collision generates a steady localized structure of even parity whose length exceeds the sum of the lengths of the individual traveling pulses. Figure 15(a) shows the details of the collision in a space-time plot, while panel (b) shows the amplitude $\mathcal{A}$, computed over the domain length $L = 80\pi$, as a function of time. The evolution is nonmonotonic as the approaching pulses alternately reinforce one another and suppress one another. The coalescence is very rapid and is accompanied by a noticeable overshoot before the solution relaxes to the final steady state.

In Fig. 16, we show an asymmetrical collision starting from two different asymmetric states, both at $r = -0.65$ and with opposite speeds. The longer state has drift speed 3.1×10^{-3}, i.e., although it has larger amplitude, it is, in fact, slower.

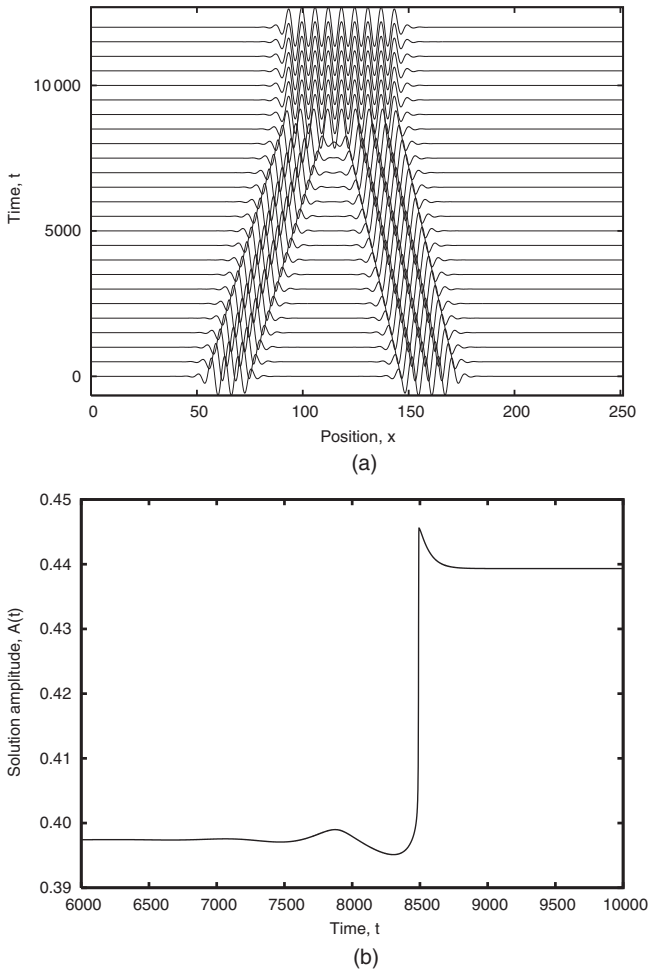

FIG. 16. (a) Interaction of two different localized states at $r = -0.65$ and $\epsilon = 0.1$, taken from the stable region of neighboring Z branches in a space-time plot. Solution profiles are separated by 500 time units. (b) Evolution of the solution amplitude $\mathcal{A}$, computed on the full domain of length 80π. The final state is a stationary even-parity localized state.

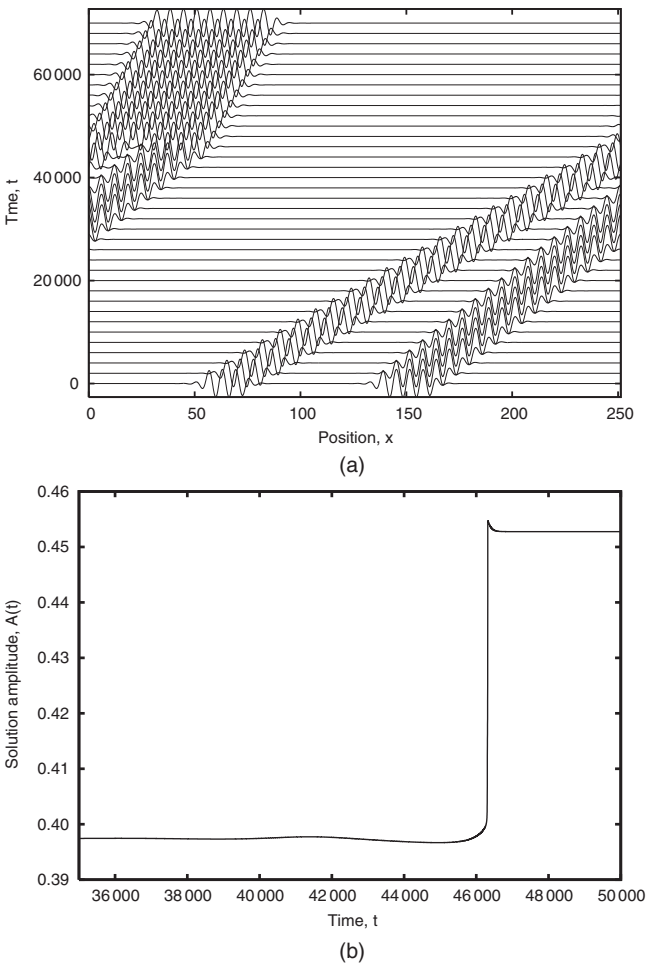

FIG. 17. As for Fig. 16, but now with both localized states traveling in the same direction, with the faster pulse behind the slower pulse. The resulting state is asymmetric and, as a result, continues to travel, albeit at a much slower speed. Successive solution profiles are separated by 2000 time units. (b) Evolution of the solution amplitude $\mathcal{A}$, computed on the full domain of length 80π.

Despite its asymmetry, the collision once again creates an even-parity stationary state that is wider than the sum of the lengths of the individual pulses. As in the preceding example, this appears to be a result of constructive interference wherein each pulse provides a sufficient perturbation to its neighbor to bump the smaller interior peaks up to the amplitude of the competing periodic state.

Figure 17 shows a collision between the two pulses in Fig. 16, but this time traveling in the same direction. The final state is an asymmetric traveling state whose length is larger than the sum of the individual lengths and, therefore, whose speed is much less than the individual speeds.

Figure 18 shows the two possible results when an asymmetric state collides with a stationary symmetric solution. In each case, the resulting state is longer than the sum of the initial profiles, with a pair of extra peaks formed in the center. Two possible outcomes have been identified, depending on the outermost fronts, i.e., the fronts not involved in the collision. When these fronts are alike (i.e., related by an approximate R symmetry), the final state is stationary and even [Fig. 18(b)]. In contrast, when these fronts are unlike (i.e., related by an approximate $\kappa \circ R$ symmetry), the final state is asymmetric and continues to drift [Fig. 18(a)].

V. DISCUSSION AND CONCLUSIONS

Homoclinic snaking in systems with reflection symmetry κ differs in a fundamental way from that present in nonsymmetric systems [11]. As shown in Fig. 19, the $L_{0,\pi}$, $L_{\pi/2,3\pi/2}$ branches in the symmetric case snake with double the frequency of the $L_{0,\pi}$ branches in the nonsymmetric case. This is a consequence of the fact that, in symmetric systems, the solutions add half a wavelength on either side in passing from a saddle node to the next saddle node above, while in nonsymmetric systems, a full wavelength is added on either side during a similar oscillation. Thus, when the symmetry κ is broken, the resulting deformation of the snakes-and-ladders structure in Fig. 1 must be such as to: (i) create two distinct braided branches of even states from the original even snaking branch, (ii) eliminate every second back-and-forth oscillation

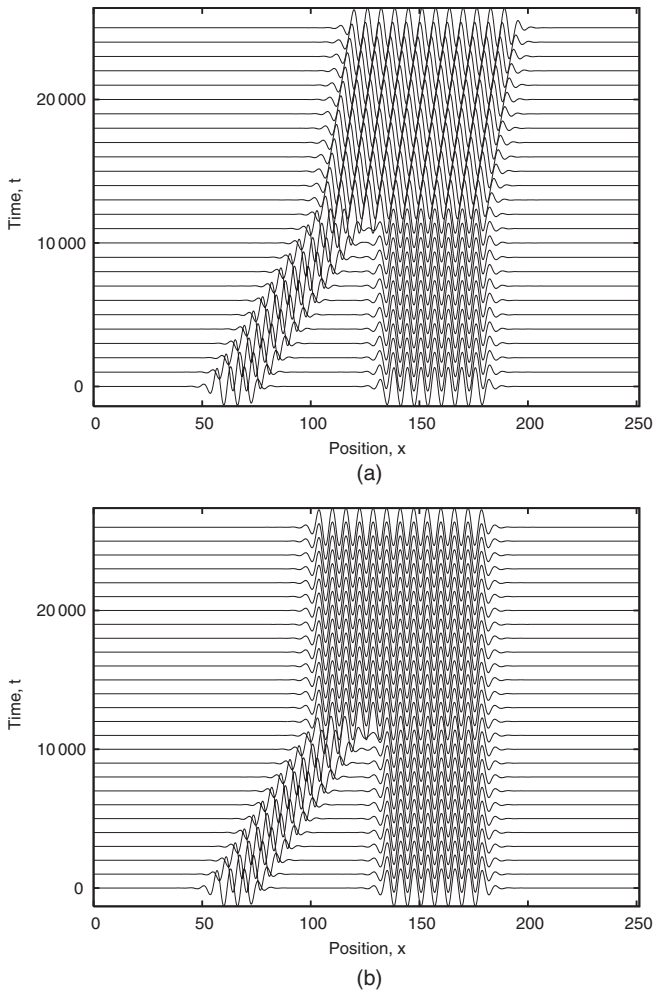

FIG. 18. Collision of a pulse from the asymmetric branch with different stationary states, (a) an L_0 state and (b) an L_π state. In both cases, $\epsilon = 0.1$ and $r = -0.65$. Solution profiles are separated by 1000 time units. In (a), the final state is asymmetric and continues to travel, albeit at a much slower speed. In case (b), the final state is symmetric and so is stationary.

of the branch together with the corresponding rung states, and (iii) replace the snaking odd-parity states and the remaining rung states by monotonic branches connecting the two braided even-parity branches.

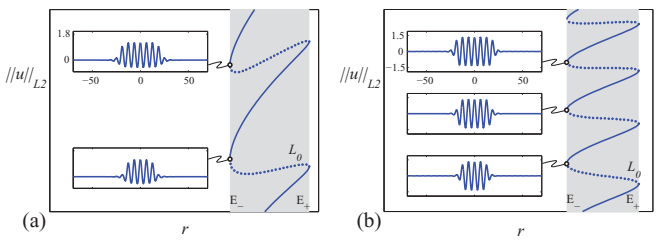

FIG. 19. (Color online) Comparison of the snakes-and-ladders structure of the pinning regions in (a) SH23, viz., $u_t = ru - (1 + \partial_x^2)^2 u + b_2 u^2 - u^3$, and (b) SH35, Eq. (1), together with sample L_0 profiles. The figure shows that, to generate a localized state of a given length, the L_0 branch executes twice as many back-and-forth oscillations in case (b) than in case (a). Parameters: (a) $b_2 = 1.8$ and (b) $b_3 = 2$. Reproduced with permission from Ref. [20].

In this paper, we have studied this process in the Swift-Hohenberg equation with competing cubic-quintic nonlinearities (SH35). Our computations reveal that breaking the symmetry κ splits the branch of even states $L_{0,\pi}$ into two branches by shifting consecutive L_0 saddle nodes alternately inward and outward relative to the κ-symmetric case and likewise for L_π but out of phase with the L_0 saddle nodes. At the same time, the $L_{\pi/2,3\pi/2}$ saddle nodes are all shifted inward, and the odd-parity states reconnect with the asymmetric states on the rungs in the snakes-and-ladders structure owing to the destruction of the parity-breaking bifurcations on the $L_{\pi/2,3\pi/2}$ branch. These reconnections result in two different disconnected branches of asymmetric states. Of these, the S branches provide connections from one even-parity branch (L_0 or L_π) to itself, while the Z-shaped branches provide connections between L_0 and L_π. With increasing asymmetry, the S-shaped connections shrink to zero, while the Z-shaped connections gradually straighten out and produce monotonic runglike connections between L_0 and L_π. Thus, for sufficiently large symmetry breaking, the snakes-and-ladders structure resembles that familiar from the Swift-Hohenberg equation with competing quadratic-cubic nonlinearities (SH23) [17]. The above process is independent of the nature of the symmetry-breaking term used and represents one of three types of snaking behavior identified in Ref. [15] on the basis of geometrical arguments. Its presence here is an inevitable consequence of the breaking of the κ symmetry, a fact that sheds new light on the occurrence of this process in physical systems.

We have emphasized that the breaking of the symmetry κ via nonvariational terms results, in general, in localized structures that drift. These structures are asymmetric and arise both from asymmetric rung states and from odd-parity states where the odd parity has been broken. Since the interaction between localized structures falls off exponentially with their separation, almost any nonvariational symmetry-breaking perturbation will destroy a bound state of odd-parity localized structures and will lead to drift of the individual pulses. We have examined various types of collisions of such pulses. These collisions lead, in general, to structures whose length exceeds the sum of the individual lengths (amalgamation), and these may be either stationary or drifting depending on the profiles (and speeds) of the individual pulses. Since short structures travel faster than long ones, the resulting collisions differ qualitatively from those common in systems supporting solitary waves in which the large amplitude wave usually travels faster than a small amplitude wave. In our case, the shorter, faster pulses do not have enough "momentum" to destroy the longer, slower pulse, in contrast, for example, to pulses described by coupled complex Ginzburg-Landau equations [21,22].

When the symmetry R is broken instead of κ, the snakes-and-ladders structure is also destroyed. Burke *et al.* [23] show, using SH23, that, in this case, the snakes-and-ladders structure breaks up into a stack of figure-eight isolas. Each isola consists of asymmetric states with a particular length, and all such states drift. Outside of the pinning region, nucleation of new cells competes with the drift of the structure leading to asymmetric nucleation. In the present problem, similar behavior is associated with convectons that drift because of the broken κ symmetry, and once again, asymmetric nucleation

is the result. However, to the right of the pinning region, repeated nucleation leads to longer and longer structures with a corresponding decrease in drift speed. Thus, the asymmetry between the nucleation fore and aft gradually decreases with increasing time. The opposite occurs to the left of the pinning region where cells are destroyed asymmetrically, and the asymmetry gradually increases with time.

We mention that S-shaped and Z-shaped secondary and tertiary branches are common in snaking scenarios. For example, such branches are generated in SH35 when periodic boundary conditions are replaced by Neumann or Dirichlet boundary conditions [24], a fact likely due to the loss of discrete translation symmetries. Such branches are also present in the snaking of multipulse states in systems with midplane reflection symmetry [3] since the presence of a second pulse breaks the κ symmetry of the first pulse. Finally, similar structures, with identical stability properties, are associated with two-dimensional structures in SH35 as well [25].

ACKNOWLEDGMENTS

This work was supported, in part, by the National Science Foundation under Grant No. DMS-0908102.

[1] O. Batiste, E. Knobloch, A. Alonso, and I. Mercader, J. Fluid Mech. **560**, 149 (2006).
[2] I. Mercader, O. Batiste, A. Alonso, and E. Knobloch, J. Fluid Mech. **667**, 586 (2011).
[3] D. Lo Jacono, A. Bergeon, and E. Knobloch, Phys. Fluids **22**, 073601 (2010).
[4] S. Blanchflower, Phys. Lett. A **261**, 74 (1999).
[5] J. H. P. Dawes, J. Fluid Mech. **570**, 385 (2007).
[6] K. Ghorayeb and A. Mojtabi, Phys. Fluids **9**, 2339 (1997).
[7] A. Bergeon and E. Knobloch, Phys. Fluids **20**, 034102 (2008).
[8] P. Assemat, A. Bergeon, and E. Knobloch, Fluid Dyn. Res. **40**, 852 (2008).
[9] H. Sakaguchi and H. R. Brand, Physica D **97**, 274 (1996).
[10] J. Burke and E. Knobloch, Phys. Lett. A **360**, 681 (2007).
[11] J. Burke and E. Knobloch, Chaos **17**, 1 (2007).
[12] P. Coullet, R. E. Goldstein, and G. H. Gunaratne, Phys. Rev. Lett. **63**, 1954 (1989).
[13] P. D. Woods and A. R. Champneys, Physica D **129**, 147 (1999).
[14] P. Coullet, C. Riera, and C. Tresser, Phys. Rev. Lett. **84**, 3069 (2000).
[15] M. Beck, J. Knobloch, D. J. B. Lloyd, B. Sandstede, and T. Wagenknecht, SIAM J. Math. Anal. **41**, 936 (2009).
[16] S. J. Chapman and G. Kozyreff, Physica D **238**, 319 (2009).
[17] J. Burke and E. Knobloch, Phys. Rev. E **73**, 056211 (2006).
[18] J. Guckenheimer and P. Holmes, *Nonlinear Oscillations, Dynamical Systems, and Bifurcations of Vector Fields* (Springer-Verlag, New York, 1986).
[19] J. Burke and J. H. P. Dawes (unpublished).
[20] J. R. Burke, Ph.D. thesis, University of California, Berkeley, 2008.
[21] H. R. Brand and R. J. Deissler, Phys. Rev. Lett. **63**, 2801 (1989).
[22] M. Iima and Y. Nishiura, Physica D **238**, 449 (2009).
[23] J. Burke, S. M. Houghton, and E. Knobloch, Phys. Rev. E **80**, 036202 (2009).
[24] J. H. P. Dawes, SIAM J. Appl. Dyn. Syst. **8**, 909 (2009).
[25] D. Avitabile, D. J. B. Lloyd, J. Burke, E. Knobloch, and B. Sandstede, SIAM J. Appl. Dyn. Syst. **9**, 704 (2010).